Journal of Chromatography A, 1554 (2018) 45–60

Contents lists available at ScienceDirect

Journal of Chromatography A

journal homepage: www.elsevier.com/locate/chroma

Evaluation of recent Protein A stationary phase innovations for capture of biotherapeutics

Timothy M. Pabst*, Johnny Thai, Alan K. Hunter

MedImmune, Purification Process Sciences, One MedImmune Way, Gaithersburg, MD 20878, USA

ARTICLE INFO

Article history:
Received 21 December 2017
Received in revised form 26 March 2018
Accepted 29 March 2018
Available online 7 April 2018

Keywords:
Protein A
Antibody
Affinity chromatography
Dynamic binding capacity
Bioprocessing

ABSTRACT

We describe a comprehensive evaluation of 12 Protein A stationary phases for capture of biotherapeutics. We first examine the morphological properties of the stationary phases using a variety of orthogonal techniques including electron microscopy, particle sizing, pressure-flow behavior, and isocratic pulse response. A panel of nine proteins spanning a wide range of structures and biochemical properties was then used to assess equilibrium uptake, mass transport, dynamic binding capacity, and elution pH. Process performance and product quality were also examined under realistic bioprocess conditions using clarified mammalian cell culture broth. Equilibrium isotherms were found to be highly favorable, with equilibrium binding capacity for monoclonal and bispecific antibodies ranging from 47–100 mg/mL packed bed across all stationary phases tested. Effective pore diffusivities, D_e, were obtained by fitting the chromatography general rate model to breakthrough data. The fitted D_e values for monoclonal antibodies ranged from 1.1–5.7 × 10^{-8} cm^2/s. The stationary phases had high dynamic binding capacities for the model proteins. The highest dynamic capacities for monoclonal and bispecific antibodies were seen with MabSelect SuRe pcc and MabSelect PrismA, which ranged from 58–74 mg/mL packed bed at 4 min residence times. Product capture using clarified cell culture broth as a feedstock showed high yields and elution pool volumes that ranged from 2–3 column volumes in most cases. Host cell protein, DNA, and aggregate levels in the elution pool were dependent on the specific nature of protein being purified, and levels were consistent between stationary phases. Lastly, we perform an analysis of bivariate correlations and discuss considerations for process design and optimization.

1. Introduction

Monoclonal antibodies (mAbs) continue to be the most prevalent class of approved biotherapeutics [1]. In addition, the use of Fc-fusion proteins and mAb-like molecules, such as bispecific antibodies and antibody-drug conjugates (ADCs), continues to increase [2–4]. Since the first mAb was approved in the 1980s, Protein A has become the most widely used capture step for Fc-containing molecules due to its highly specific nature, ease of use, and strong regulatory track record. For these purification processes, Protein A chromatography is routinely utilized as part of a platform approach where it is placed first in the purification train to capture product from clarified cell culture broth [5–13]. This configuration allows for robust processing of similar molecules. Even with these advantages, there have been efforts to identify alternatives to Protein A, such as cation exchange or multimodal capture chromatography, to overcome the burden of high stationary phase costs [14–19]; however, these techniques may not be as selective and may lack the ability to be employed as part of a platform approach. There has also been interest in non-chromatographic techniques, such as precipitation [20–22] and aqueous two-phase extraction [23–25], but these strategies have not gained widespread use for industrial-scale bioprocessing. Thus, it seems unlikely that Protein A chromatography will be superseded as the dominant platform approach for antibody and Fc-fusion protein purification in the foreseeable future, and its use is likely to continue to increase with the growth in the market [26].

Staphylococcal Protein A is a 42 kDa single chain polypeptide located on the outer surface of *Staphylococcus aureus* [27–30]. Early Protein A affinity stationary phases consisted of native Protein A coupled to a base matrix most often through covalent bonding to amines. Since then, dramatic improvements have been made in Protein A chromatography stationary phases, most notably increased stability under alkaline conditions realized through point

* Corresponding author.
E-mail address: pabstt@medimmune.com (T.M. Pabst).

https://doi.org/10.1016/j.chroma.2018.03.060

Nomenclature

c	interstitial protein concentration (mg/mL)
C	protein concentration in solution (mg/mL)
C_F	column protein feed concentration (mg/mL)
c_p	protein concentration in the pore fluid (mg/mL)
CCCB	clarified cell culture broth
CV	column volume (mL)
d_p	volume mean particle diameter (μm)
D_{ax}	axial dispersion coefficient (cm^2/s)
D_e	effective pore diffusivity, $=\varepsilon_p D_p$ (cm^2/s)
D_p	pore diffusivity (cm^2/s)
D_0	free solution diffusivity (cm^2/s)
DBC	dynamic binding capacity (mg/mL)
EBC	equilibrium binding capacity (mg/mL)
K	adsorption constant in Langmuir isotherm model (mL/mg)
k_f	film mass transfer coefficient (cm/s)
K_D	distribution coefficient, $=\left(V_R/CV-\varepsilon_b\right)/(1-\varepsilon_b)$
L	bed height (cm)
M	dextran molecular weight (Da)
q	stationary phase protein concentration (mg/mL)
q_d	percent of total in a histogram particle size bin (%)
q_m	maximum binding capacity in Langmuir isotherm model (mg/mL)
r	radial coordinate (cm)
r_p	volume mean particle radius (μm)
r_{pore}	pore radius (nm)
r_s	dextran hydrodynamic radius (nm)
t	time (s)
S	standard error of regression (units of the response variable)
u	superficial mobile phase velocity (cm/s)
v	interstitial mobile phase velocity (cm/s)
V_R	retention volume (mL)
$V_{10\%}$	volume at which 10% breakthrough occurs (mL)
z	axial coordinate (cm)

Dimensionless numbers

N_{Bi}	Biot number, $=k_f r_p/D_e$
N_{Re}	Reynolds number, $=d_p u\rho/\mu\varepsilon_b$
N_{Sc}	Schmidt number, $=\mu/\rho D_0$

Greek symbols

ΔP	pressure drop in a packed bed (MPa)
ε_b	extraparticle porosity (interstitial column volume fraction)
$\varepsilon_{p,x}$	intraparticle porosity for solute x
ε_T	total column porosity, $=\varepsilon_b+(1-\varepsilon_b)\varepsilon_p$
μ	dynamic viscosity (cP)
ρ	density (g/mL)

mutations in the B and C domains of Protein A [31]. Many of the commercially available Protein A stationary phases now consist of engineered ligands with repeat units derived from the B or C domain, and can withstand many cycles of exposure to sodium hydroxide concentrations at or greater than 0.1 N.

In addition to the increase in alkaline stability, there has been a robust demand to increase the binding capacity of Protein A stationary phases in response to continuously increasing cell culture titers, which now routinely exceed 5 g/L. Process models developed to predict facility capacity and cost of goods have been shown to be sensitive to Protein A capture column dynamic binding capacity (DBC) [32,33]. Moreover, the importance of increased binding capacity, both equilibrium and dynamic capacity, is not limited to batch processing as similar increases in productivity are expected in continuous multi-column process settings. In response to these market pressures, numerous Protein A stationary phases have been introduced over the last several years to achieve ever higher DBCs and increased productivity. In some cases, an increase in DBC is realized by improving static binding capacity through modification of the ligand [34,35] or increasing the ligand density [7,36]. In other cases, DBC can be increased by reducing mass transfer resistance such that the available static capacity is utilized more efficiently [37–40].

In this work, we examine recent innovations in Protein A stationary phases suitable for industrial-scale capture of biopharmaceuticals. The work includes comprehensive characterization of the stationary phase morphological properties, as well as binding and elution behavior for a panel of antibodies and Fc-fusion proteins. In addition, we quantitatively describe protein mass transfer using the general rate model to determine effective pore diffusivity. Finally, the Protein A stationary phases were tested with clarified cell culture broth to assess process performance and product quality under realistic bioprocess settings.

2. Materials and Methods

2.1. Buffer reagents and protein preparations

Chemicals used for buffer preparation and dextran standards were obtained from Sigma (St. Louis, MO, USA) and JT Baker (Phillipsburg, NJ, USA). Antibodies and Fc-fusion proteins were expressed in Chinese hamster ovary (CHO) cells using standard cell culture techniques. To generate purified material, clarified cell culture broth was purified by Protein A chromatography and then by ion exchange chromatography. Table 1 summarizes the antibodies and Fc-fusion proteins used in this work.

2.2. Protein A stationary phases

Protein A stationary phases used in this work are summarized in Table 2 along with publicly available data obtained from manufacturer literature. All stationary phases were commercially available, except for MabSelect PrismA, which was obtained as a pre-commercial launch sample from GE Healthcare (Marlborough, MA, USA). The Protein A stationary phases were flow packed in 1.1 cm diameter Vantage L11 columns from Millipore (Billerica, MA, USA) to a 10 cm bed height and compression factors of ~1.2 were achieved for all resins. Packed bed quality was evaluated by calculating asymmetry factors and reduced HETP from pulses of sodium chloride in Tris buffer at pH 7.4. Values for asymmetry factor ranged from 1.0–2.2 and reduced HETP values ranged from 3.6–9.2, which are consistent with the reduced HETP values recently reported for lab-scale columns [41].

2.3. Protein concentration determination

Protein concentrations of purified samples were determined using a Nanodrop 2000c from Thermo Scientific (Wilmington, DE, USA) with the microvolume pedestal and measurement at a wavelength of 280 nm. Concentrations of antibodies and Fc-fusion proteins in clarified cell culture broth were determined by analytical Protein A high-performance liquid chromatography (ProA-HPLC) using a POROS A 20 (4.6 mm ID × 10 cm, 20 μm) column obtained from Thermo Fisher (Grand Island, NY, USA) with an Agilent 1200 HPLC system (Palo Alto, CA USA). The HPLC system was operated at 3.5 mL/min with binding and elution mobiles phases consisting of phosphate buffered saline (PBS) at pH 7.2 and pH 2.2, respectively. Samples were applied to the column

Table 1
Protein properties.

Molecule	Class	pI[a]	MW (kDa)[b]	r_h(nm)[c]	D_0 (x10^{-7} cm^2/s)[d]
mAb1	Antibody (IgG1)	8.3–9.0	146.7	5.2	4.6
mAb2	Antibody (IgG4)	6.9–7.5	147.3	5.3	4.5
mAb3	Antibody (IgG1)	7.8–8.4	149.0	5.4	4.5
bsAb1	Bispecific Ab (IgG1-(scFv)$_2$)	8.9–9.1	206.2	6.3	3.8
bsAb2	Bispecific Ab (IgG1-(scFv)$_2$)	8.8–9.0	204.6	6.0	4.0
bsAb3	Bispecific Ab (IgG1-(peptide)$_2$)	8.0–8.7	158.7	5.8	4.2
Fc1	Fc fusion (IgG4Fc-(ligand)$_2$)	7.0–8.3	159.0	5.4	4.5
Fc2	Fc fusion ((IgG4Fc)$_3$-(ligand)$_6$)	5.6–6.5	310.0	8.1	3.0
Fc3	Bispecific Fc fusion (IgG4-(ligand)$_2$)	6.1–7.7	280.0	7.4	3.3

[a] Measured by capillary isoelectric focusing.
[b] Measured by mass spectrometry including contribution from glycosylation.
[c] Calculated by Stokes-Einstein equation with D_0 measured by dynamic light scattering at infinite dilution.
[d] Measured by dynamic light scattering at infinite dilution.

Table 2
Protein A stationary phase properties as reported by manufacturers.

Name	Abbreviation	Manufacturer	Base matrix	Protein A ligand progenitor domain (number of repeat units)	d_p (μm)	Alkaline stabilized
MabSelect SuRe	MSS	GE Healthcare	Agarose	B (4)	85	Yes
MabSelect SuRe LX	LX	GE Healthcare	Agarose	B (4)	85	Yes
MabSelect SuRe pcc	PCC	GE Healthcare	Agarose	B (4)	50	Yes
MabSelect PrismA	PrismA	GE Healthcare	Agarose	B (6)	~60	Yes
Amsphere A3	A3	JSR Life Sciences	polymethacrylate	–[a]	50	Yes
AF-rProtein A HC-650F	650F	Tosoh Biosciences	polymethacrylate	C (6)	45	Yes
KanCapA	KCA	Kaneka	Cellulose	C (5)	65-85	Yes
KanCapA 3G	KCA3G	Kaneka	Cellulose	–[a]	65-85	Yes
Eshmuno A	EshA	EMD Merck	Polyvinylether	C (5)	~50	Yes
Praesto AP	AP	Purolite	Agarose	–[a]	85	Yes
Monofinity A	MonoA	Genscript	Agarose	–[a]	~90	Yes
MabSpeed rP202	rP202	Mitsubishi	polymethacrylate	C (–[a])	45	Yes

[a] Not disclosed by the manufacturer.

neat and the elution profile was monitored at 280 nm using the system spectrophotometer. Elution peak area was converted to protein concentration using a standard curve generated with purified material.

2.4. Aggregate determination by size exclusion HPLC

Aggregate levels in purified protein samples were determined by analytical high-performance size exclusion chromatography (SEC-HPLC) using a TSKgel G3000SW$_{XL}$ (7.8 mm ID × 30 cm, 5 μm) column obtained from Tosoh Biosciences (King of Prussia, PA, USA) with an Agilent 1260 HPLC system. The HPLC system was operated at 1 mL/min with a mobile phase consisting of 100 mM sodium phosphate, 200 mM sodium sulfate, pH 6.8. The mobile phase used to analyze mAb1 samples also included 10% isopropanol. Samples (250 μg) were applied to the column neat and the elution profile was monitored at 280 nm using the system spectrophotometer. Aggregate levels were determined as a ratio of peak areas of the early-eluting aggregate peak(s) and the monomer peak.

2.5. Dynamic Light Scattering

Dynamic light scattering (DLS) measurements were made with a DynaPro Plate Reader II from Wyatt Technology (Santa Barbara, CA, USA) with purified protein samples prepared at 2–10 g/L in 25 mM Tris, 150 mM NaCl, pH 7.4. 35 μL protein samples were measured in triplicate in 384 well plates at 20 °C. Diffusivities were obtained from the Dynamics software (version 7.4.0) and hydrodynamic radii were calculated within the software using the Stokes-Einstein equation. Averaged (n = 3) values were plotted versus concentration and extrapolated to obtain diffusivity values and hydrodynamic radii at infinite dilution.

2.6. Electron microscopy

Transmission electron microscopy (TEM) of stationary phases was performed at Charles River Pathology Associates (Durham, NC, USA). Stationary phases in their shipping solutions (~20% ethanol) were dehydrated with graded steps to 100% ethanol, solvent exchanged into 100% acetone, and then embedded in Spurr's resin to generate solid sample blocks. Thin sections (~90 nm) were cut using a diamond knife, stained with methanolic uranyl acetate and Reynold's lead citrate, and then examined with a transmission electron microscope from JEOL (Peabody, MA, USA; model JEM-1011). TEM was performed at magnifications between 800–6000x and high-resolution images were captured with an AMT XR16M digital camera.

2.7. Particle size measurements

Volume mean diameters were determined by light scattering using the Partica laser scattering particle size distribution analyzer (model LA-950V2) from Horiba Instruments (West Chicago, IL, USA). Stationary phase samples were prepared at 15% slurries in 50 mM Tris, 150 mM NaCl, pH 7.4 and then 1 mL of the sample slurry was added to the detection chamber and measured at room temperature. Horiba software reported the volume mean diameter, the standard deviation of the particle size distribution, and the distribution histogram. Samples were measured in triplicate and the volume mean diameter was determined from the average of three sample measurements.

2.8. Pressure-flow curves

Pressure drop across packed beds was measured at linear superficial velocities between 0–400 cm/h using a digital manometer

(model 3462) purchased from Traceable Products (Webster, TX, USA). Column inlets were connected to an AKTA Pure 25 (GE Healthcare, Marlborough, MA USA) system pump and the column outlet left open to atmospheric pressure. The digital manometer was connected to the inlet and outlet tubing with T-connections. Pressure drop measured in an empty column with the adapters pushed together was subtracted from the packed bed measurements.

2.9. Particle porosity measurements

Particle porosities, ε_p, were obtained from isocratic pulses injections of mAb3, bsAb1, and sodium chloride carried out at 150 cm/h using an AKTA Pure 25. For protein pulses, the mobile phase was 50 mM acetate, 100 mM NaCl, pH 3.0 for all protein and stationary phase combinations except proteins injected on to the Toyopearl AF-rProteinA HC-650F column, which used 100 mM acetic acid to prevent interactions with the column at pH 3.0. Protein samples (final concentration ~2.5 mg/mL) were injected on to the columns using a 100 μL sample loop. For sodium chloride injections, the mobile phase was 50 mM Tris, 150 mM NaCl, pH 7.4, and 100 μL samples of 50 mM Tris, 1 M NaCl, pH 7.4 were injected using a sample loop. Peak retention was monitored using the AKTA instrumentation (absorbance for proteins, conductivity for sodium chloride) and the data was exported to Excel software to determine the peak retention volume using the first statistical moment. The system volume, determined in an empty column with the adapters pushed together, was subtracted from the values obtained in packed beds.

2.10. Inverse size exclusion chromatography using dextran pulse injections

Dextran injections were carried out at 1 mL/min using an Agilent 1260 HPLC and the peak retention was monitored with an Agilent refractive index (RI) detector (Model G1362A). The mobile phase (50 mM Tris, pH 7.4) was controlled to 26 °C with a recirculating water bath. Temperature of the autoinjector, column block, and RI detector were controlled at 26 °C using Chemstation software. Dextran samples, purchased from Sigma-Aldrich (with nominal molecular weights of 10 kDa (catalog #D9260), 40 kDa (31389), 70 kDa (31390), 270 kDa (00894), 410 kDa (00895), and 670 kDa (00896), and dextrose, purchased from Thermo Fisher Scientific (catalog #D16-1), were dissolved in the mobile phase buffer at a final concentration of 5 mg/mL and injected neat (10 μL) on to the ~10 mL Protein A columns (packed in Vantage L11 columns as described previously). Data was exported to Excel software to determine the peak retention volume, V_R, using the first statistical moment, and the distribution coefficient, $K_D = \left(V_R/CV - \varepsilon_b\right)/(1-\varepsilon_b)$. Peaks were normalized by peak area for plotting. The system volume, determined in an empty column with the adapters pushed together, was subtracted from the values obtained in packed beds.

2.11. Adsorption isotherms

Equilibrium adsorption isotherms were constructed from 1.25 mL batch binding experiments. Protein stock solutions were prepared at ~5 mg/mL in equilibration buffer (50 mM Tris, 150 mM NaCl, pH 7.4) and diluted to known concentrations with equilibration buffer in 1.5 mL Eppendorf tubes. Stationary phase slurries were prepared at ~15% in equilibration buffer, added to the diluted protein samples, and allowed to gently mix on a rotator for 24–28 hours. After equilibration, the Eppendorf tubes were centrifuged briefly to pellet the stationary phases and the protein concentrations in the liquid phases were measured. A mass balance was used to determine the amount of protein that was bound to the stationary phase at equilibrium.

2.12. Breakthrough behavior and equilibrium binding capacity measurements

Breakthrough behavior was determined using the AKTA Pure 25 at a residence time of 4 minutes with a ~10 mL packed bed. Purified protein load was adjusted to pH 7.4 ± 0.2 and conductivity was adjusted to 15 ± 2 mS/cm with sodium chloride. The column was equilibrated with 50 mM Tris, 150 mM NaCl, pH 7.4 and then loaded with protein (feed concentration, C_F ~5 mg/mL) until the column was saturated (i.e. the outlet concentration was ~99% of the feed concentration). The exact protein concentration of the feed was determined by offline A280 measurement using the Nanodrop 2000c. Bed exhaustion occurred with a protein load of 150–225 mg/mL column volume, depending on the protein and stationary phase. Instantaneous concentration at the column outlet was measured online at 280 nm using the AKTA UV meter. The UV absorbance was measured with the column in bypass to determine the maximum absorbance of the protein feed solution. To test for linearity, the AKTA UV meter was calibrated with mAb1, which had the greatest UV absorbance of the proteins evaluated in this study. A highly linear calibration curve was obtained over the protein concentration range used for breakthrough and dynamic binding capacity experiments.

The equilibrium binding capacity (EBC, in mg/mL of solid support) was determined from a full breakthrough curve by numerically integrating the area above the curve and below the feed concentration according to:

$$\mathrm{EBC} = \frac{\int_0^\infty (C_F - C)dV - \varepsilon_T C_F CV}{(1-\varepsilon_T)CV} \quad (1)$$

Where $\varepsilon_T = \varepsilon_b + (1-\varepsilon_b)\varepsilon_P$ is the total porosity (outside of particle and inside pores), ε_b is the extraparticle porosity, and CV is the column volume (or packed bed volume). In this equation, the integral in the numerator represents the mass of protein accumulated in the column during the entire breakthrough experiment and the second term in the numerator represents the mass of protein that remains unbound in the liquid within the column; taken together they represent the mass of protein bound to the solid phase during the experiment. The denominator represents the amount of stationary phase (in units of mL of solid support). The system holdup volume (determined by protein pulses in empty columns with the adapters pushed together) was also subtracted from the volume loaded. EBCs were converted to mg/mL of particle or mg/mL of packed bed using ε_p and ε_b, as appropriate.

2.13. Dynamic binding capacity measurements

Dynamic binding capacity (DBC), defined as the amount of protein loaded at 10% breakthrough, was determined for stationary phases packed in ~10 mL columns using an AKTA Pure 25 in a manner similar to full breakthrough curves as described above. The column was equilibrated with 50 mM Tris, 150 mM NaCl, pH 7.4 and then loaded with pH and conductivity adjusted purified protein at C_F ~5 mg/mL until >10% breakthrough was observed. DBC was determined at residence times of 2.4, 4, and 6 minutes according to:

$$\mathrm{DBC} = \frac{(V_{10\%} - \varepsilon_T CV)C_F}{CV} \quad (2)$$

where $V_{10\%}$ is the volume at which 10% breakthrough occurs.

As can be seen from Eq. (2), the unbound protein that remains in the liquid inside the column is subtracted from the bound protein for purposes of calculating DBC, whereas the amount of protein that

Table 3
Summary of Protein A stationary phase morphological properties.

Name	Particle size[a] (μm)		r_{pore}[b] (nm)	Extraparticle porosity, ε_b[c]	Intraparticle porosity			
	d_p	SD			$\varepsilon_{p,mAb3}$[d]	$\varepsilon_{p,bsAb1}$[d]	$\varepsilon_{p,NaCl}$[e]	$\varepsilon_{p,dex}$[b]
MabSelect SuRe	89.6	21.8	41.8	0.31	0.76	0.70	0.96	0.94
MabSelect SuRe LX	88.4	20.7	38.2	0.31	0.69	0.65	0.96	0.90
MabSelect SuRe pcc	44.4	6.5	29.7	0.35	0.57	0.53	0.92	0.87
MabSelect PrismA	54.1	8.1	32.7	0.34	0.50	0.49	0.94	0.92
Amsphere A3	49.6	8.4	46.0	0.34	0.61	0.53	0.89	0.85
AF-rProtein A HC-650F	54.2	7.2	30.8	0.34	0.36	0.30	0.91	0.76
KanCapA	75.0	11.7	51.0	0.36	0.67	0.69	0.98	0.91
KanCapA 3G	79.2	11.3	42.5	0.33	0.70	0.69	0.95	0.88
Eshmuno A	50.2	8.1	40.8	0.34	0.74	0.70	0.82	0.81
Praesto AP	92.5	20.8	37.4	0.25	0.69	0.64	0.95	0.95
Monofinity A	95.7	20.3	36.8	0.29	0.63	0.60	0.98	0.92
MabSpeed rP202	44.9	5.7	60.5	0.37	0.42	0.44	0.86	0.74

[a] As measured by laser light scattering. d_p is the volume mean diameter; SD is the standard deviation of the frequency distribution.
[b] Determined by fit of Eq. (4) to isocratic elution data obtained with dextran probes ranging from 10–670 kDa.
[c] Determined from fit of Eq. (3) to pressure drop data in a packed bed.
[d] Determined from injections of mAb or bsAb under non-binding (acidic) conditions described in Section 2.9.
[e] Determined from NaCl pulse injections.

breaks through the column (up to 10% breakthrough) is included in the DBC value. A more rigorous calculation, like Eq. (1) where the limits of integration go from 0 to $V_{10\%}$, could be implemented to account for protein that breaks through up to $V_{10\%}$, but this contribution is negligible and thus was not accounted for in the DBC values. The total porosity determined by mAb3 injections was used in DBC calculations for mAb1-3, bsAb1, and Fc1 (i.e. the smaller proteins), while total porosity determined by bsAb1 injections was used for the larger proteins.

2.14. Linear pH gradient elution chromatography

For linear pH gradient elution experiments, columns were equilibrated with 50 mM Tris, 150 mM NaCl, pH 7.4 and then purified protein was loaded on the column to 5 mg/mL packed bed using an AKTA Pure 25. The column was re-equilibrated, washed with 50 mM citrate, pH 6.7, and then eluted in a linear gradient to 50 mM citrate, pH 2.7 over 10 column volumes at 150 cm/h. Equilibration and elution buffer pH was measured offline using a SevenMulti pH meter from Mettler Toledo (Columbus, OH, USA) equipped with an InLab Expert Pro pH probe from Mettler Toledo and calibrated with pH 2, 4, 7, and 10 standards. Peak retention volume was determined by peak maximum absorbance (from the AKTA spectrophotometer at 280 nm). Elution pH at the peak maximum was calculated through linear interpolation between the offline pH values of the two buffers used to form the gradient. The AKTA pH trace was adjusted to account for the total column porosity, ε_T, and the system delay volume. Elution pH at peak maximum as determined by linear gradient elution was used to select an appropriate elution pH for the step elution phase in the capture chromatography experiments described in the following section.

2.15. Capture from clarified cell culture broth

Capture of proteins from clarified cell culture broth (CCCB) was evaluated in packed columns using an AKTA Pure 25. Columns were equilibrated with 50 mM Tris, 150 mM NaCl, pH 7.4 and then CCCB was loaded on the column at a residence time of 4 min. The load was calculated as 85% of the DBC measured at a residence time of 4 min. Columns were re-equilibrated with 50 mM Tris, 150 mM NaCl, pH 7.4 and then eluted in stepwise fashion with 25 mM acetate, pH 3.4–3.5 for all stationary phases except for Toyopearl AF-rProteinA HC-650F (which used pH 3.2), and MabSpeed rP202 (pH 3.8). Elution pools were collected from 100-100 mAU (using AKTA spectrophotometer with a 2 mm path length at 280 nm). Step yield was determined using mass of product in the load (determined by ProA-HPLC) and pool (determined by A280).

2.16. Host cell protein and DNA measurements

Host cell protein (HCP) concentrations were measured using the bioaffy sandwich immunoassay on the Gyrolab xP workstation from Gyros AB (Uppsala, Sweden). Capture and detection antibodies were in-house reagents raised against HCP from the cell line used to produce the antibodies and Fc-fusion proteins used in this work.

Host cell DNA concentrations were measured by an in-house method employing a sodium iodide/sodium dodecyl sulfate/Proteinase K sample treatment followed by an isopropanol DNA extraction coupled with a quantitative Polymerase Chain Reaction targeting the Short Interspersed Nuclear Element DNA sequence repeated across the CHO genome with SYBR Green based detection.

3. Results and discussion

3.1. Stationary phase morphological properties

Table 3 summarizes Protein A stationary phase morphological properties. As can be seen in the table, particle sizes were in agreement with data provided by the manufacturer and standard deviations measured were typically small compared to the mean particle size (13–24% of the volume averaged mean value). Particle size distributions can be found in Supplemental material (Fig. S3). Extraparticle porosities of the stationary phases packed in chromatography columns were determined by fitting the Kozeny equation [42] to pressure drop data (by minimizing the residual sum of squares):

$$\frac{\Delta P}{L} = 150\frac{\mu}{d_P^2}\frac{(1-\varepsilon_b)^2}{\varepsilon_b^3}u \quad (3)$$

Where μ and u are the mobile phase dynamic viscosity and superficial velocity, respectively, and d_P is the average particle diameter. For this work, d_P-values determined from particle sizing (volume mean diameters; see Table 3) were used in place of manufacturer's data. Pressure drop curves were found to be linear over the range tested (up to 400 cm/h in 1.1 cm × 10 cm packed beds) and the magnitude of the pressure drop was consistent with expectations based

on particle size. It is worth noting that the pressure drop in a larger diameter manufacturing-scale column will likely be higher due to a loss of wall support; nonetheless, the data presented is useful to assess relative differences between the stationary phases. The fitted ε_b-values are shown in Table 3 and pressure drop curves with the fitted Kozeny equation are shown in Supplemental material (Fig. S4).

Particle porosities measured using sodium chloride were greater than 0.9 for the less rigid (agarose and cellulose) particles and between 0.8–0.9 for the more rigid (synthetic polymer) particles suggesting a higher percentage of solids in the base matrices for the synthetic polymer supports. Particle porosity was also estimated with mAb3 and bsAb1 under non-binding (acidic) conditions. As expected, the larger proteins could not access the entire pore volume due to steric restrictions, and resulted in porosities that were lower than obtained using sodium chloride, with only minor differences observed between the mAb ($\varepsilon_{p,mAb3}$ = 0.34–0.76) and the slightly larger bsAb ($\varepsilon_{p,bsAb1}$ = 0.30–0.70) as shown in Table 3.

Inert dextan probes, ranging from 10–670 kDa, were used to further elucidate particle porosity (data in Supplemental material, Fig. S5). For all the stationary phases tested, the largest 670 kDa dextran probe could access a limited fraction of the particle volume while smaller dextran probes gained access to a larger portion of the particle volume. To estimate the pore radius, r_{pore}, and intraparticle porosity, $\varepsilon_{p,dex}$, using the dextran elution data, a cylindrical pore model was applied according to Hagel et al. [43]:

$$K_D = \varepsilon_{p,dex}\left(1 - \frac{r_s}{r_{pore}}\right)^2 \tag{4}$$

Where K_D is the distribution coefficient and r_s is the dextran hydrodynamic radius. For this work r_s-values were estimated from the dextran viscosity radii correlation of Squire [44]:

$$r_s = 0.028 \times M^{0.47} \tag{5}$$

where M is the dextran molecular weight. A plot of $\sqrt{K_D}$ vs. r_s was used to obtain the fitted values of r_{pore}, and $\varepsilon_{p,dex}$ (by linear least squares). The $\varepsilon_{p,dex}$-values obtained, as shown in Table 3, were slightly higher than those of non-retained proteins and slightly lower than those obtained using sodium chloride injections, suggesting that the dextran probes experience a macroporous structure free of very small pores that only sodium chloride can access. The r_{pore}-values obtained from the model fit, as shown in Table 3, were generally consistent across stationary phases, with values in the range of 30–60 nm. These data suggest that the particles have highly porous structures which was supported by TEM of the stationary phases (data in Supplemental material, Fig. S2).

TEM micrographs showed spherical particles with well-connected porous networks, regardless of the base matrix material. Some differences were observed in the morphology of the base matrix structures, where the more rigid synthetic polymer materials appeared to have structures that include dense nodes surrounded by pore networks, but in general the pore sizes appeared to be similar, which is consistent with the cylindrical pore model results discussed above.

Substantial variation in staining was observed across the stationary phases as shown in Fig. S2. For example, Monofinity A and MabSelect PrismA appeared to be heavily stained while MabSelect SuRe pcc and Praesto AP showed little staining. The stains employed in this study, uranyl acetate and Reynold's lead citrate, are primarily utilized for TEM imaging of biological specimens. Exactly how they interact with embedded stationary phase specimens of this nature remains a matter of conjecture. Therefore, while heavier staining implies a region with a higher concentration of electron dense atoms, it is difficult to draw conclusions beyond this. In particular, we would caution against interpretations that link staining variation to Protein A ligand density or distribution under the assumption that these stains primarily interact with the polypeptide chain of the Protein A ligand.

3.2. Adsorption isotherms

Fig. 1 shows adsorption isotherms for mAb1 on Protein A stationary phases. Adsorption isotherms for all other protein and stationary phase combinations are available in Supplemental material (Fig. S6). The isotherm data were fit with the Langmuir isotherm:

$$q = \frac{q_m K C}{1 + KC} \tag{6}$$

where q_m is the maximum binding capacity and K is the adsorption constant. Fitted values of these parameters (determined by minimizing the residual sum of squares) are available in Supplemental material (Table S2). Since there are challenges in the isotherm experimentation, particularly with accurate determination of stationary phase volume added to the isotherm batch binding experiment, we adopted a methodology that relies on breakthrough experiments to estimate q_m-values in a manner similar to Ng et al. and Reck et al. [45–47]. The q_m-value (and corresponding experimental q-values shown in Fig. 1 and Fig. S6) were normalized to the EBCs ascertained with Eq. (1) using full breakthrough curves such that q_m is set equal to the EBC. This approach assumes for Eq. (6) that $q = q_m$ at $C = C_F$, which is valid for the case of a nearly rectangular isotherm provided that C_F lies in the flat portion of the curve. In most instances, the q_m-value changed by less than 15% when normalizing to the EBC value.

As can be seen in Fig. 1 (and Supplemental material Fig. S6) the isotherms are highly favorable for all stationary phases, which is consistent with Protein A behavior previously reported in the literature [37,39,40]. Equilibrium capacities are quite high for the Protein A stationary phases, greater than 140 mg/mL particle in some instances. To make comparisons within the large data set, EBCs of stationary phases were averaged for a given stationary phase across various protein groupings (e.g. all of the mAbs, or all of the proteins with molecular weights in the range of 147–159 kDa). Comparing stationary phases in terms of average EBC value for proteins with molecular weights similar to mAbs, MabSelect PrismA and MabSelect SuRe pcc performed best, averaging >126 mg/mL particle. KanCapA 3G and MabSelect SuRe LX showed the next highest equilibrium capacities (107–112 mg/mL particle), followed by Toyopearl AF-rProteinA HC-650F, Monofinity A, and Praesto AP (92–96 mg/mL particle), and then Amsphere A3, MabSpeed rP202, and Eshmuno A (81–86 mg/mL particle). Similar capacities and trends were observed for the larger bsAbs (~200 kDa); however, average EBCs for the larger Fc-fusion proteins (280–310 kDa) were 50-65% of the those determined for the smaller proteins.

3.3. Dynamic binding capacity

Dynamic binding capacities at 10% breakthrough were determined for all combinations of proteins and stationary phases for 2.4, 4, and 6 min residence times. Fig. 2 shows DBC plotted as a function of residence time. DBC values are also available in tabular format in Supplemental material (Table S1). For the 4 min residence time condition, full breakthrough curves were obtained for columns loaded to 150–220 mg/mL packed bed, and are shown in Fig. 3 for mAb1. Full breakthrough curves at 4 min residence time for the remaining molecule and stationary phases combinations are available in Supplemental material (Fig. S7).

As can be seen in Fig. 2, the Protein A stationary phases have high dynamic binding capacities, greater than 70 mg/mL packed bed in some instances at 4–6 min residence times. The range of

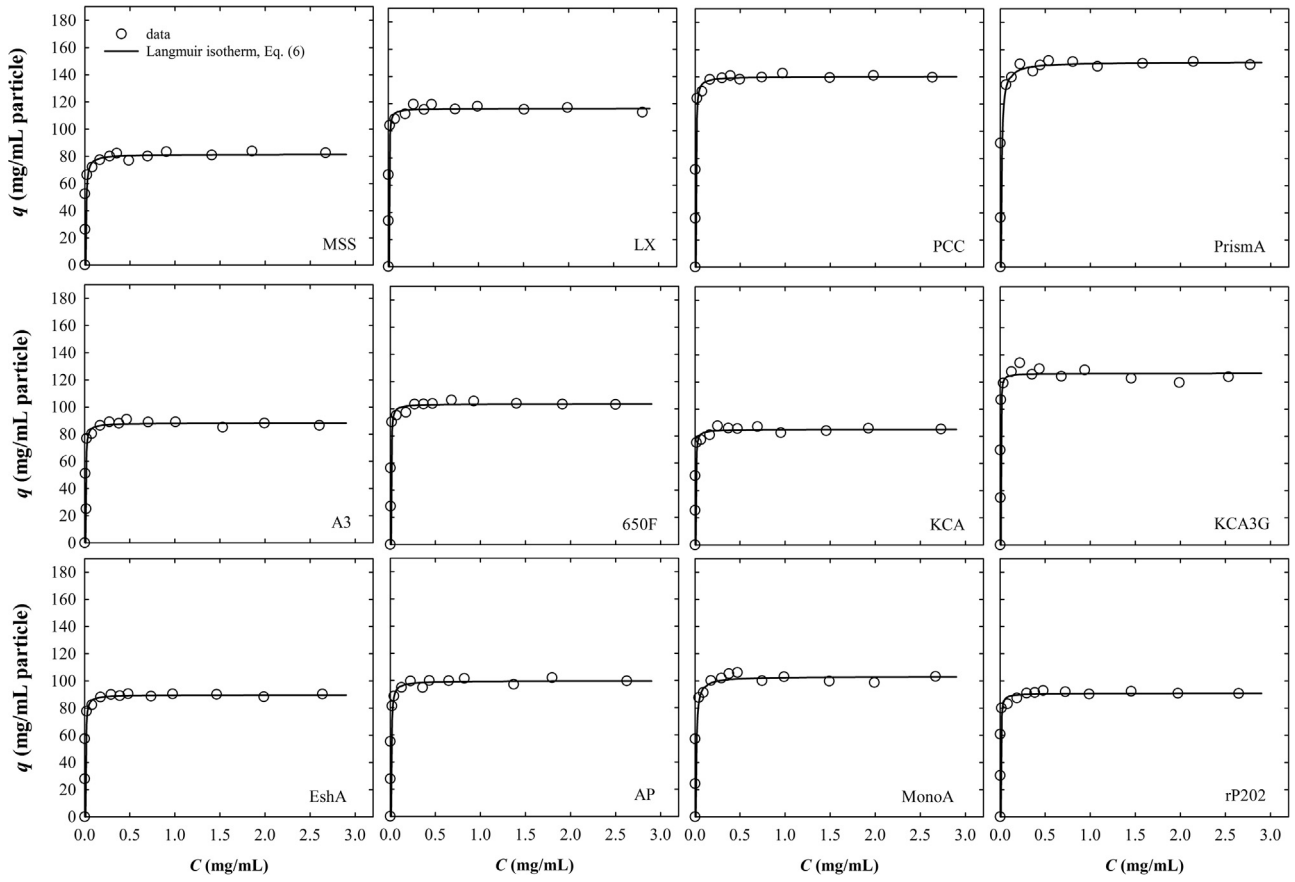

Fig. 1. Equilibrium isotherms for mAb1 on Protein A stationary phases. Open circles are experimental data and the solid line is a fit of the Langmuir isotherm, Eq. (6), with parameters given in Table S2.

dynamic binding capacities that were observed was similar for the mAbs and bsAbs except for mAb1, which was higher for all stationary phases. For Fc1, which is similar in size to the mAbs, the DBC range was broader across stationary phases, but largely similar to mAbs and bsAbs. For the larger Fc2 and Fc3 molecules, the binding capacities were considerably lower, reaching 30-40% of the capacity determined for the smaller mAbs and bsAbs.

Similar to the analysis of EBC in the previous section, comparisons were made between stationary phases in terms of average DBC at 4 min residence time for proteins with molecular weights similar to mAbs (147–159 kDa). The stationary phases generally fell into groups with MabSelect PrismA and MabSelect SuRe pcc having the highest DBCs for all molecules at 4 minutes residence time. The next group of stationary phases included KanCapA 3G, MabSelect SuRe LX, Toyopear AF-rProtein A HC-650F, Praesto AP, and Amsphere A3, while the remaining stationary phases behaved similarly to each other in a third group. For larger bsAbs (~200 kDa) and the larger Fc-fusion proteins (~300 kDa) the average DBC comparison groupings remained the same but Amsphere A3 and Toyopearl AF-rProtein A HC-650F moved to the top of the second group while MabSelect SuRe LX and KanCapA 3G fell slightly within the second group. This observation suggests that Amsphere A3 and Toyopearl AF-rProtein A HC-650F may be able to better accommodate the larger proteins.

In all cases, the DBC data follow the expected trend where shorter residence times resulted in lower dynamic binding capacities. The decrease in DBC between 6 min and 4 min residence times was consistent for mAbs and bsAbs and was typically smaller than the decrease from 4 min to 2.4 min. Comparing stationary phases for a given molecule revealed that MabSelect PrismA, Monofinity A, MabSelect SuRe LX, KanCapA 3G, and Praesto AP were slightly more sensitive to residence time, as these stationary phases showed steeper declines in DBC between 4 min and 2.4 min residence times across most proteins tested. The larger impact of residence time suggests these resins may experience higher mass transfer resistance. This topic is explored in the next section.

3.4. Protein mass transport

Mass transfer plays a key role in the performance of modern Protein A stationary phases [36–39]. Therefore, examination of protein mass transport is crucial to gain a comprehensive understanding of these materials and make informed judgements. To characterize protein mass transport in packed beds, we chose the chromatography general rate model, given by:

$$\frac{\partial c}{\partial t} = -\nu\frac{\partial c}{\partial z} + D_{ax}\frac{\partial^2 c}{\partial z^2} - \frac{1-\varepsilon_b}{\varepsilon_b}\frac{3}{r_p}k_f(c - c_{p|r=r_p}) \tag{7}$$

$$\frac{\partial c_p}{\partial t} = D_p\left(\frac{\partial^2 c_p}{\partial r^2} + \frac{2}{r}\frac{\partial c_p}{\partial r}\right) - \frac{1-\varepsilon_p}{\varepsilon_p}\frac{\partial q}{\partial t} \tag{8}$$

Eq. (7) represents a mass balance on the interstitial column volume with terms for convection, dispersion, and film mass transfer. Eq. (8) represents a mass balance on the stationary phase with terms for pore diffusion and adsorption.

Danckwerts boundary conditions were applied at the column inlet and outlet [48]. A symmetry condition was assumed at the bead center, and stagnate film mass transfer was applied at the boundary of the stationary phase and the interstitial column volume [48]. Local equilibrium was assumed for protein adsorption as

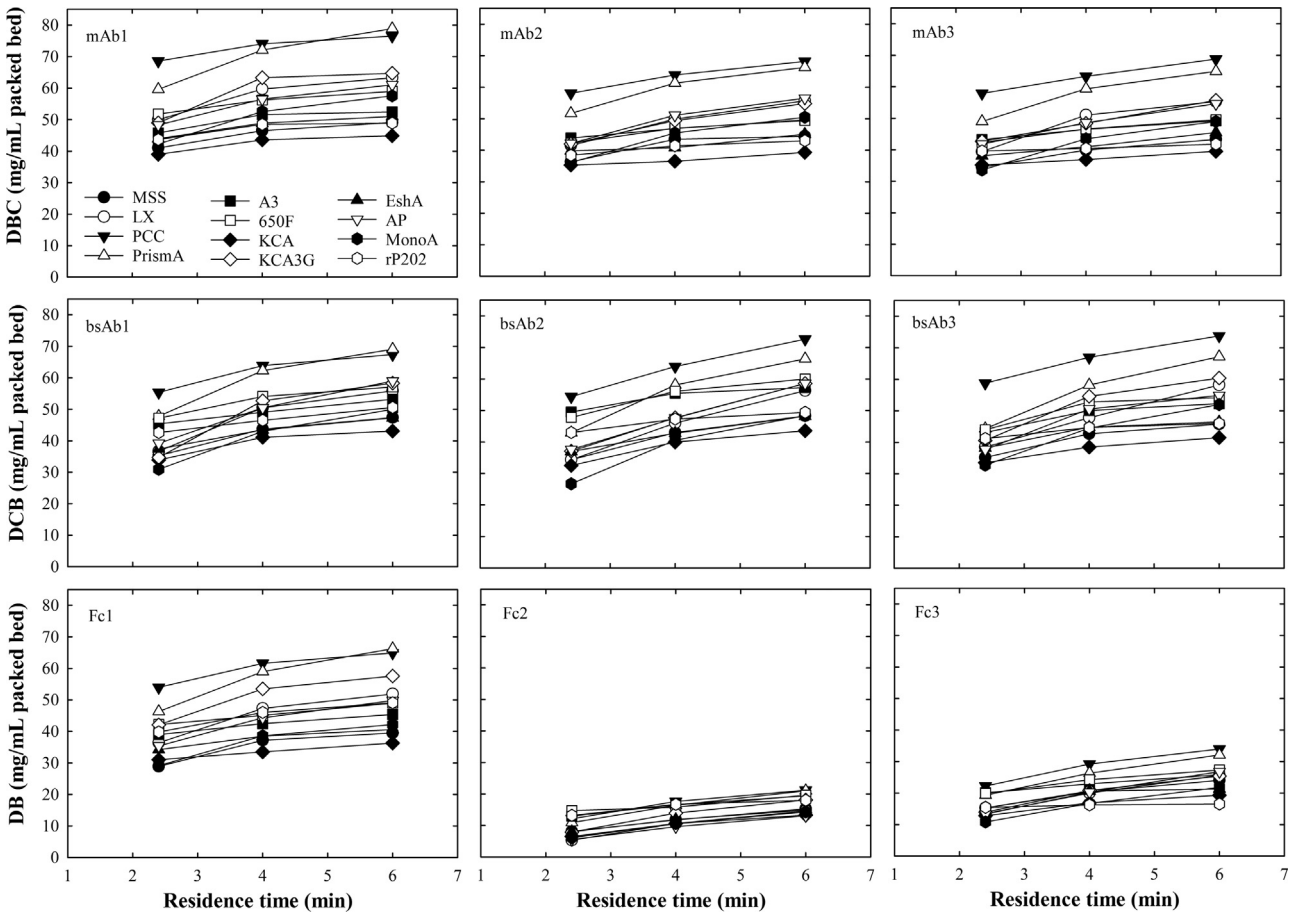

Fig. 2. Dynamic binding capacities as a function of residence time for mAbs, bispecific antibodies, and Fc fusion proteins on Protein A stationary phases.

described by Eq. (6). Equations (7), (8) and the boundary conditions were spatially discretized using finite volumes and the weighted essentially non-oscillatory (WENO) method [48]. The resulting system of ordinary differential equations was numerically integrated using CADET software version 2.3.2 (64 bit) running on a Windows 7 PC with MATLAB version R2014b and an Intel CORE i7 CPU [49].

Langmuir isotherm parameters, K and q_m, are given in Supplemental materials (Table S2). Axial dispersion, D_{ax}, was neglected [50,51]. The particle radius, r_p, extraparticle porosity, ε_b, and particle porosity, ε_p, were obtained from Table 3. $\varepsilon_{p,mAb3}$ was used for the smaller proteins (mAb1-3, bsAb3, and Fc1), and $\varepsilon_{p,bsAb1}$ was used for the larger proteins (bsAb1-2, Fc2-3). The film mass transfer coefficient, k_f, was estimated from the correlation given by Carberry [52]:

$$k_f = 1.15\frac{u}{\varepsilon_b}N_{Re}^{-1/2}N_{Sc}^{-2/3} \tag{9}$$

Where $N_{Re} = d_p u\rho/\mu\varepsilon_b$ (Reynolds number) and $N_{Sc} = \mu/\rho D_0$ (Schmidt number).

Using the parameter values described above, pore diffusivity, D_p, was fit to experimental breakthrough data by minimizing the residual sum of squares (RSS). Fig. 3 shows modeling results obtained for mAb1. As can be seen from the figure, the goodness of fit was generally excellent in this case but did vary from stationary phase to stationary phase. Other proteins (shown in Supplemental material Fig. S6) tended to behave similarly. Perhaps not surprisingly, overall a better fit was obtained with the mAbs and a poorer fit was obtained with the larger Fc-fusion proteins.

When the goodness of fit was inferior it was associated with instances where the breakthrough curve tailed to a greater extent, suggesting a slow approach to equilibrium. This observation is confirmed quantitatively by the standard error of regression, S, also shown in Fig. 3 (and Fig. S6 in Supplemental material). The tailing behavior has previously been explained based on a heterogeneous binding mechanism where there are fast binding sites that are diffusion controlled and slow sites controlled by binding kinetics [39].

In the context of Protein A, this explanation intuitively makes sense as there are multiple binding sites on a single Protein A ligand [7,34]. We can speculate that the diffusion controlled fast binding sites correspond to low binding occupancy of a Protein A ligand. On the other hand, as ligand occupancy increases, we can surmise that the remaining binding sites may become less accessible and more sterically hindered, corresponding to slow binding kinetics. Therefore, in instances where this behavior was observed, the reported effective pore diffusivity, D_e ($=\varepsilon_p D_p$), value essentially represents an average that incorporates resistances due to both pore diffusion and binding kinetics, likely having limited predictive usefulness. Nonetheless, even when the goodness of fit varied, the D_e-values obtained were often consistent. For example, based on both quantitative measures (S) and qualitative comparison, the goodness of fit spanned a broad range for the three mAbs on MabSelect SuRe LX. Despite this, the D_e-values obtained by minimization of RSS varied relatively little, ranging from $3.0–3.5 \times 10^{-8}$ cm^2/s, which is probably within the expected error for this type of measurement.

Fig. 4 summarizes D_e/D_0 for all proteins and stationary phases evaluated in this study. Quantitative values of all results summarized in Fig. 4 are provided in Supplemental material (Table S2). D_0 values are summarized in Table 1 and DLS data used to estimate D_0 are given in Supplemental material (Fig. S1). Where available, the D_e-values obtained were largely consistent with

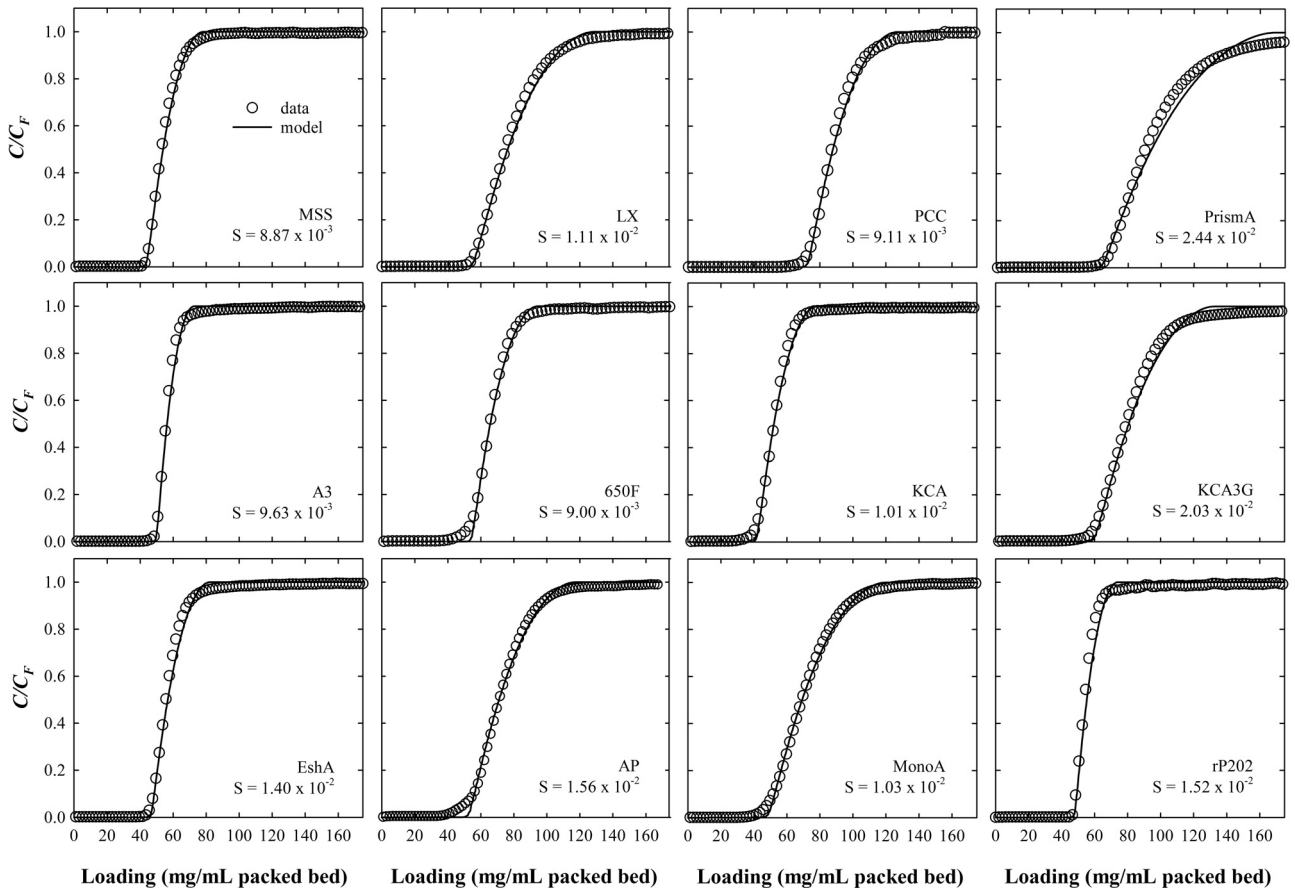

Fig. 3. Breakthrough curves for mAb1 on Protein A stationary phases. Open circles show experimental data and solid lines show fitted model results based on Eqs. (7) and (8) using parameters in Table S2. The standard error of regression, S, is given for each stationary phase.

previously reported values for Protein A stationary phases evaluated at higher protein concentrations [36,38,39]. In particular, the D_e-values obtained in this study for monoclonal antibodies at 5 mg/mL concentration on MabSelect SuRe, which ranged from 4.8–5.7 $\times$ 10^{-8} cm^2/s, were in good agreement with values reported by Hahn and coworkers [38]. In their detailed study, a D_e-value of 5×10^{-8} cm^2/s was obtained for shallow bed uptake on MabSelect SuRe at 3.0 mg/mL protein concentration. With respect to external mass transfer, the Biot Number (N_{Bi}) values obtained across all stationary phases and proteins tested ranged from 118-990, suggesting film mass transfer plays a negligible role under the conditions utilized for this study.

3.5. Linear pH gradient elution chromatography

Since Protein A chromatography is often employed as part of a platform approach, it is important to select an elution pH that works consistently for a majority of the modalities to be purified with the platform process. This may include more than one antibody format as well as Fc-fusion proteins. Table 4 summarizes the elution pH determined by pH gradient elution for all protein and stationary phase combinations. As can be seen in the table, elution pH was found to occur between 3.5–3.8 and only minor variations were observed for all molecules on a given stationary phase. There were a few exceptions to this behavior that were specific to a protein or stationary phase. For example, Toyopearl AF-rProtein A HC-650F required the lowest pH for elution of all proteins (0.1–0.3 pH units lower), while the elution pH for MabSpeed rP202 was found to be higher than the other stationary phases (0.2–0.5 pH units higher). This unique high pH elution on MabSpeed rP202 could be beneficial for proteins that are sensitive to acidic conditions, such as Fc-fusion proteins, which can aggregate rapidly under acidic conditions [53]. The only protein that was out of trend was Fc3 which was found to elute 0.3–0.4 pH units higher than all other proteins. This data set was used to select an appropriate elution pH for the step elution conditions used for purification of select molecules from clarified cell culture broth. In most cases pH 3.4–3.5 was suitable for step elution; however, AF-rProtein A HC-650F required a lower pH (pH 3.2) while MabSpeed rP202 could elute the select molecules with a higher pH (pH 3.8).

Based on previous reports in the literature, the underlying cause of the observed variation in elution pH, and in the milder elution conditions seen for MabSpeed rP202 in particular, are most likely due to ligand polypeptide sequence differences as a result of protein engineering to improve ligand performance [54]. This remains a matter of speculation; however, as Protein A ligand sequence information for the stationary phases evaluated in this study have not been publicly disclosed by the manufacturers. Nonetheless, similar strategies have demonstrated it is possible to elute Protein A under milder pH conditions through destabilization of the ligand itself or the ligand-Fc interaction [55–57].

3.6. Capture from clarified cell culture broth

Capture chromatography experiments were conducted to test the ability of the Protein A stationary phases to selectively purify three of the proteins in this study. In all cases, the chromatogram for the capture step was well behaved, showing sharp elution peaks and little to no protein in the 0.1 M acetic acid column strip (Fig. S8 in Supplemental material shows example chromatograms for the

Table 4
Elution pH on Protein A stationary phases as determined by pH gradient elution.

Stationary phase	pH at elution peak max								
	mAb1	mAb2	mAb3	bsAb1	bsAb2	bsAb3	Fc1	Fc2	Fc3
MabSelect SuRe	3.7	3.6	3.7	3.7	3.7	3.7	3.7	3.6	4.0
MabSelect SuRe LX	3.7	3.6	3.7	3.7	3.7	3.7	3.6	3.6	4.0
MabSelect SuRe pcc	3.7	3.6	3.7	3.7	3.7	3.7	3.6	3.6	4.0
MabSelect PrismA	3.8	3.5	3.7	3.7	3.6	3.7	3.7	3.6	4.0
Amsphere A3	3.7	3.5	3.7	3.6	3.6	3.7	3.6	3.6	3.9
AF-rProtein A HC-650F	3.4	3.4	3.5	3.5	3.5	3.4	3.2	3.3	3.7
KanCapA	3.7	3.6	3.7	3.7	3.7	3.6	3.6	3.5	3.9
KanCapA 3G	3.8	3.7	3.8	3.8	3.8	3.7	3.6	3.6	3.9
Eshmuno A	3.7	3.7	3.7	3.8	3.7	3.7	3.6	3.6	4.0
Praesto AP	3.6	3.5	3.6	3.5	3.5	3.6	3.6	3.5	3.8
Monofinity A	3.7	3.7	3.7	3.7	3.7	3.7	3.7	3.6	4.0
MabSpeed rP202	4.2	4.1	4.2	4.2	4.2	4.0	4.0	3.9	4.7

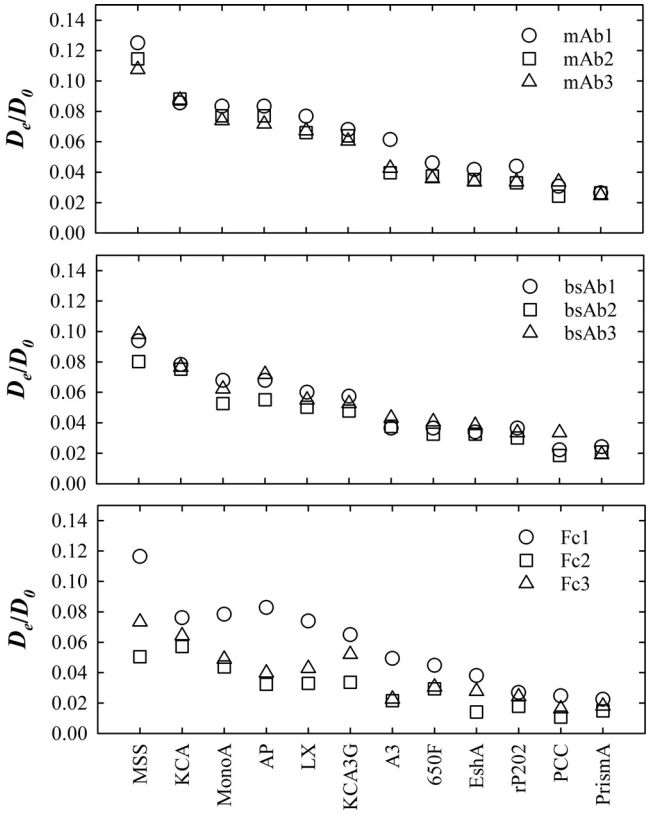

Fig. 4. D_e/D_0 values for mAbs (top panel), bsAbs (middle panel), and Fc-fusion proteins (bottom panel) measured on Protein A stationary phases. D_e-values obtained from fit of breakthrough curves using Eqs. (7) and (8) with parameters given in Table S2. D_0-values determined by DLS are given in Table 1.

capture of mAb1 from CCCB). Fig. 5 summarizes the process performance and resulting product quality in the Protein A elution pool. As can be seen in the figure, yields were consistently above 90%, with only minor differences observed between stationary phases. Elution pool volumes were slightly more variable, falling between 1.8–3.8 column volumes; however, the variability was the result of a few protein and stationary phase combinations, and most of the results fall in a narrower range of 2–3 column volumes. In some cases, higher binding capacity stationary phases did have larger elution pools compared to the lower capacity stationary phases, but no trends among high capacity resins were observed.

Protein A chromatography is most often employed as the capture column in a purification train and is expected to provide highly selective binding while process-related impurities remain in the column flow through. Moreover, Protein A chromatography is not expected to reduce the level of product-related impurities, such as aggregates, under typical operating conditions. As can be seen in Fig. 5, HCP, DNA, and aggregate levels in the elution pool were relatively consistent between stationary phases for a given protein with only minor exceptions. When considering HCP levels in the elution pool, there was no stationary phase that provided the best HCP removal for all three molecules tested. For example, MabSelect SuRe LX had the highest HCP level of all stationary phases tested for mAb1, but the lowest for bsAb3. Similarly, Toyopearl AF-rProtein A HC-650F had the lowest HCP for mAb1, but the highest for mAb3. For DNA clearance, no trends were observed; however, Monofinity A fared the best of all the stationary phases for all three proteins tested. When comparing aggregate levels for mAb1 and mAb3 in the elution pool across stationary phases, only small differences are seen, whereas more variability was observed for the aggregate level in the bsAb3 pools. Moreover, some trends in the bsAb3 data can be seen where higher (Amsphere A3) or lower (MabSpeed rP202) aggregate levels were observed in elution pools that had higher or lower protein concentrations, respectively (concentration data not shown).

When making comparisons between proteins, it was observed that some proteins are not as easily purified from CCCB, and higher levels of process- and product-related impurities are seen. Aside from the exceptions noted above, impurity levels were quite consistent when comparing stationary phases and no trends were observed based on stationary phases properties (e.g. higher binding capacity vs. lower binding capacity; natural vs. synthetic polymeric backbone materials) or process performance data (e.g. yield, pool volume, pool concentration). It should be noted that the capture purification experiments in this work only employed a re-equilibration step (50 mM Tris, 150 mM sodium chloride, pH 7.4); however, a more stringent wash is often employed to reduce non-specific interactions of HCP and stationary phases and/or HCP and the protein of interest [58–60]. It is unclear if a more stringent wash would benefit one stationary phase over another, but it is plausible that this could occur and may merit investigation when developing a Protein A capture step.

3.7. Bivariate correlation analysis

Fig. 6 shows a matrix of bivariate scatterplots correlating stationary phase morphological properties with protein binding and mass transfer. The scatterplot matrix was generated using the gplotmatrix function in MATLAB version R2014b. The diagonal shows univariate histograms with the highest frequency bin normalized to full scale on the ordinate axis. Plots in the upper left-hand quadrant are sparser as they correlate morphological properties to other morphological properties. Similar to the approach described in protein mass transport above, $\varepsilon_{p,mAb3}$ was

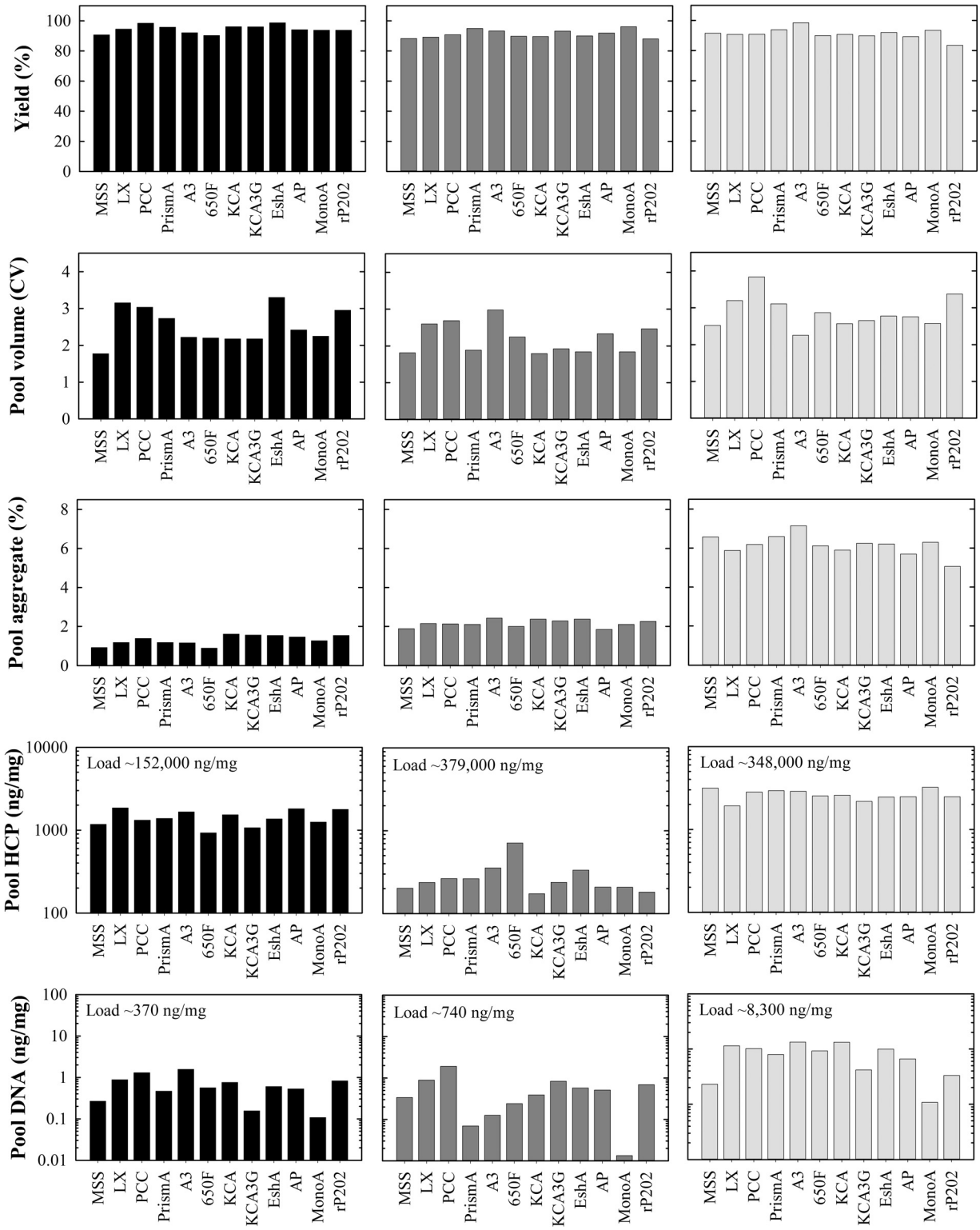

Fig. 5. Process performance and product quality obtained from capture of clarified cell culture broth for mAb1 (left panels), mAb3 (center panels), and bsAb3 (right panels) on Protein A stationary phases.

used for the smaller molecules (mAb1-3, bsAb3, and Fc1), and $\varepsilon_{p,bsAb1}$ was used for the larger molecules (bsAb1-2, Fc2-3).

Examining Fig. 6, it becomes apparent that EBC and DBC at 4 min residence time show the only strong correlation. Linear least squares analysis of this bivariate scatter plot yields an R^2 value of 0.81 with a slope of 0.70 DBC/EBC. That EBC and DBC are well correlated for such a diverse group of stationary phases and proteins suggests that different manufacturers have identified a similar optimum of DBC as a fraction of total EBC utilization. This fraction is represented by the slope of the line (0.70 DBC/EBC), meaning approximately 70% of the available equilibrium binding capacity is utilized at 4 min residence time. The fitted slope obtained by lin-

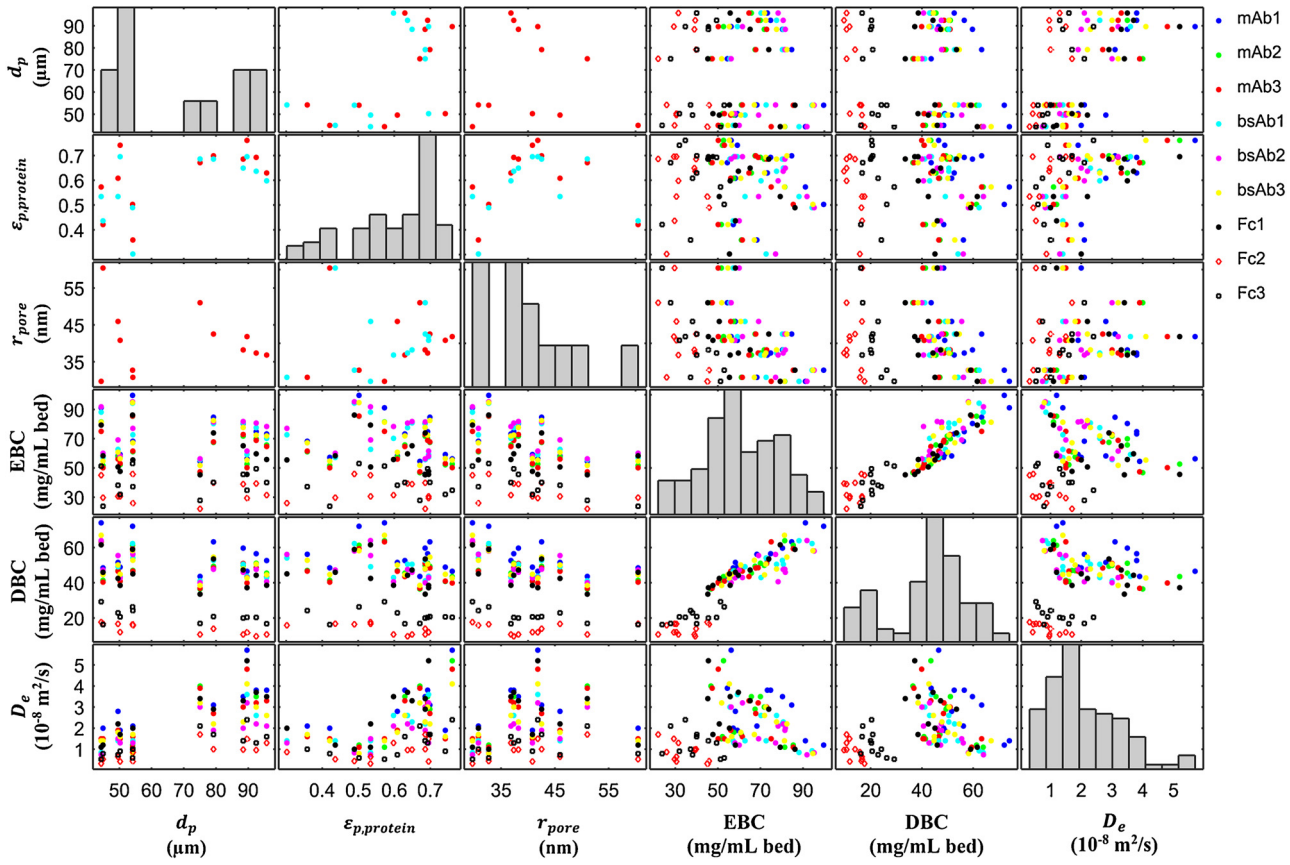

Fig. 6. Matrix of bivariate scatterplots correlating stationary phase morphological properties with protein binding and mass transfer. The diagonal shows univariate histograms with the highest frequency bin normalized to full scale on the ordinate axis.

ear least squares was in good agreement with the average value of DBC/EBC for the entire dataset, which was calculated to be 0.68.

Lastly, as shown in the lower left-hand corner of Fig. 6, a subtler correlation was identified for D_e-values with particle size. For stationary phases with a particle diameter <60 µm, the average D_e-value for all proteins tested was 1.3×10^{-8} cm²/s. On the other hand, for stationary phases >60 µm in diameter, the average D_e-value was more than double at 2.9×10^{-8} cm²/s. This result further highlights the complex balance that must be struck between mass transport rates and other competing properties. In this case, smaller bead sizes compensate for slower mass transfer. This may come at the expense of higher column back pressure at a given flow rate. As discussed by Müller and Vajda [35] and Hahn et al. [38], the results of this study show that as advances are made in base matrix properties enabling a more favorable pressure-flow relationship and hence use of smaller bead sizes, other aspects of stationary phase design likely capitalize on these improvements to achieve optimal performance. The complex nature of this optimization challenge is elucidated further in the next section.

3.8. Considerations for process optimization and stationary phase lifetime

Optimization of the Protein A capture step is critically important to increase process productivity and reduce cost of goods for manufacturing. Productivity, defined as the amount of product purified per unit time per unit column volume, is dependent on a complex interplay of numerous parameters. For example, a Protein A cycle may be optimized subject to the constraint that the entire unit operation not exceed a specified length of time (e.g. a production shift or within the specified CCCB hold time). Alternatively, column volume may be minimized to reduce stationary phase and raw material costs. The extent to which a process can be optimized is often heavily dependent on facility fit constraints such as available column sizes, tank volumes, and skid capabilities. The optimization strategy and parameter weightings are also likely to be different for clinical versus commercial manufacturing.

Fig. 7 shows the impact of residence time on DBC for mAb1 and column pressure on MabSelect SuRe LX, KanCapA 3G, MabSelect PrismA, and Amsphere A3. These high capacity stationary phases represent a diverse mix of properties likely to impact process performance, including mass transfer rates ($1.2–3.5 \times 10^{-8}$ cm²/s), particle size (50–90 µm), and base matrix material (synthetic vs. natural polymers). In the figure, experimentally determined DBC at 2.4, 4, and 6 min residence times are shown with predicted DBC for a 20 cm packed bed length constructed using the chromatography general rate model and input parameters as described in Section 3.4, with the exception of diffusivity values which were obtained from Table S2. As can be seen in Fig. 7, the model accurately predicts DBC within a few percent of the experimental data and captures the salient features of the DBC curve with a steep decrease at lower residence times.

When optimizing Protein A productivity, a compromise is often made between increasing mobile phase velocity to minimize cycle time at the expense of DBC. Several groups have published models for Protein A productivity as a function of residence time; given similar assumptions and constraints, these models show maximum productivity at residence times less than 1.5 minutes for batch processing [40,61,62]. Similar residence time ranges have also been reported as optimal for continuous or semi-continuous processing

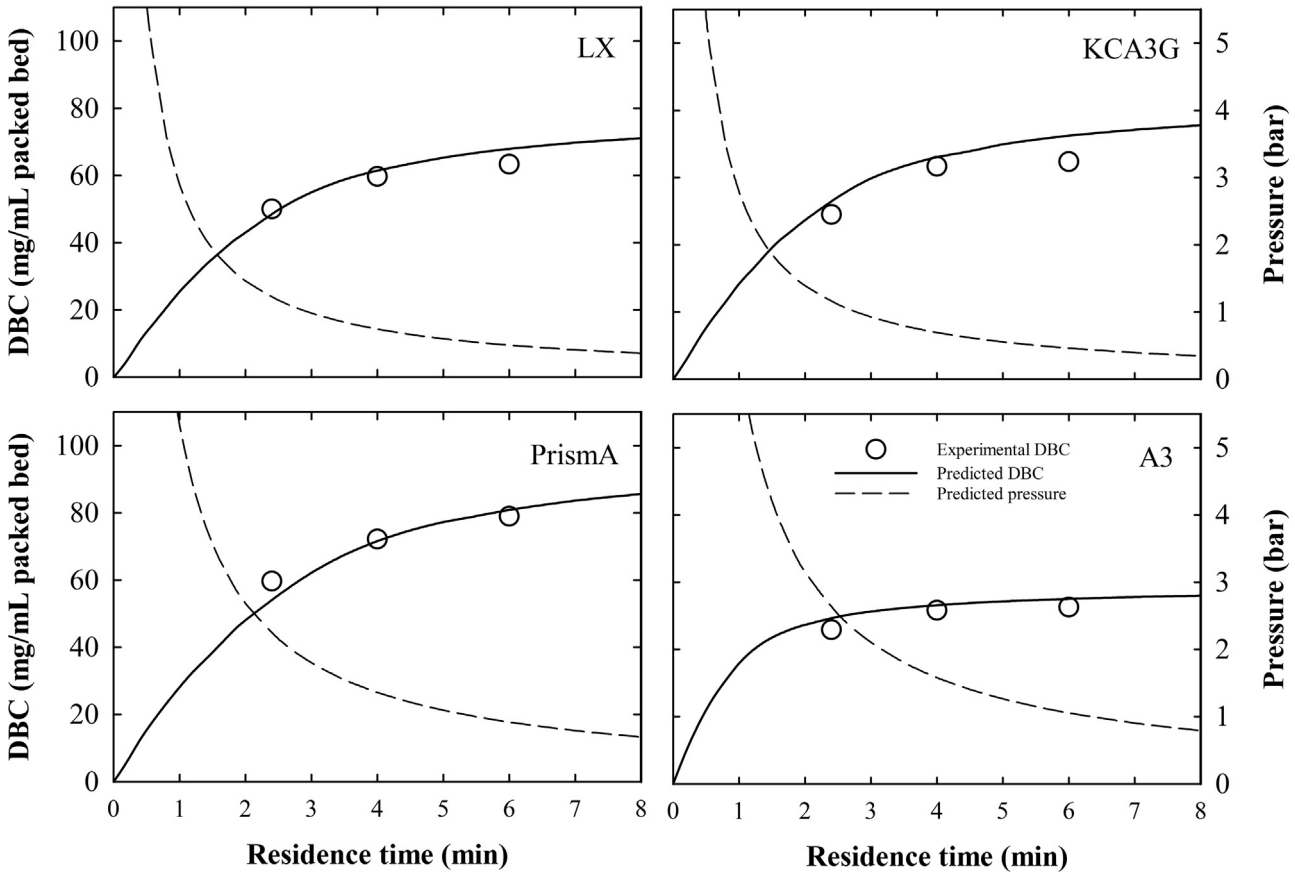

Fig. 7. Column DBC and pressure curves as a function of residence time. Experimental DBC values obtained from Table S1. Predicted DBC curves constructed using the chromatography general rate model to simulate breakthrough behavior with a 20 cm packed bed length; input parameters as described in Section 3.4, and diffusivity values obtained from Table S2. Predicted pressure curves were constructed using Eq. (3) with parameters given in Table 3 for a 20 cm packed bed length.

[46,63]. Examining Fig. 7, it is apparent that operating at residence times between 1–2 min lies in a region where DBC changes rapidly in a nonlinear fashion. Comparing DBC at 1 and 2 min residence times, Amsphere A3 showed a DBC increase of 11 mg/mL packed bed, while the other three stationary phases saw increases of 18–22 mg/mL packed bed.

Fig. 7 also displays the column pressure predicted by Eq. (3) with parameters given in Table 3. The equation assumes a linear relationship between flow rate and pressure, which is acceptable for the small-scale columns used in this work; however, this assumption becomes invalid for semi-rigid media as the column is scaled-up and loses wall support. It is worth noting that while the pressure-flow relationship shown on Fig. 7 is linear with flowrate, it is non-linear with residence time. When operating at process-scale with much larger diameter columns, the pressure-flow curve will to shift to the right, potentially limiting the maximum operational flow rate and hence productivity [61,64–66]. Additional constraints may be imposed due to the specific nature of the manufacturing facility and equipment, such as pressure rating on process-scale equipment and increases in viscosity for chilled manufacturing suites. Moreover, certain Protein A operations may be susceptible to higher viscosity during elution due to phase separation behavior at locally high concentration [67].

To overcome these limitations, packed bed height can be reduced. However, given the constraint of a fixed column diameter, this will reduce the column volume likely increasing the number of column cycles, which is unattractive due to an increase in fixed processing time for steps such as equilibration and cleaning. If column size is not a constraint, it may still be unattractive to increase diameter as large columns often require permanent installation in a manufacturing suite and will also increase capital equipment costs. Regardless of the assumptions and constraints, given that both DBC and pressure are likely to change rapidly and nonlinearly over the residence time range of interest, optimization models are expected to be very sensitive to relatively small variations in these parameters. In particular, as stationary phase manufacturers trend toward smaller bead sizes to overcome mass transport limitations, the pressure-flow relationship will have a greater influence on optimization outcomes. Therefore, to fully answer the question of optimal Protein A process design, in addition to results presented in this work, high quality pressure-flow data from process-scale columns combined with predictive models for packed beds of semi-rigid media are also necessary to reach a fundamentally sound conclusion [61,64–66].

In most commercial bioprocess scenarios, it is understood that the cost of Protein A must be distributed over numerous individual lots to reduce manufacturing costs to an acceptable level. Even when good stationary phase lifetime is achieved, often exceeding 150 cycles, cost of goods for manufacturing is usually more sensitive to Protein A capture column costs when compared to other purification process unit operations. Other groups have studied performance of Protein A stationary phases during column cycling, reporting lower DBC and yield, increased elution pool volumes, as well as increased impurity levels in the Protein A elution pool [68–73]. In general, the loss of chromatographic performance was attributed to damage to the ligand under alkaline conditions or fouling of the resin by proteinaceous material. Therefore, the cleaning and sanitization protocols employed play a crucial role in

obtaining acceptable stationary phase lifetime. Nevertheless, ligand stability and the ability to clean Protein A stationary phases after repeated exposure to CCCB is beyond the scope of this work as it is heavily dependent on the specific nature of the protein of interest, composition of the CCCB feedstock (e.g. complex vs chemically defined cell culture media), process hardware, and operating conditions chosen.

To elucidate stability under alkaline conditions, data provided by the manufacturers can shed light on the potential loss of DBC. Under standard cleaning conditions (0.1 N sodium hydroxide with 15 minutes of contact time per cycle is common), manufacturers evaluated in this study claim minimal loss of DBC over stationary phase lifetime and low levels of leached Protein A ligand in subsequent cycles. MabSelect PrismA is currently the only example where the manufacturer suggests routine cleaning with up to 1 N sodium hydroxide while showing minimal loss of DBC and low levels of ligand leaching up to 175 cycles. In many cases, the cycling data provided by manufacturers is performed under artificial settings in the absence of CCCB, and the loss of DBC is strictly a function of the loss of (or damage to) the base labile Protein A ligand. In a more realistic bioprocess scenario where the Protein A stationary phase is subjected to repeated cycling with a cruder feed stream, one must also consider fouling of the stationary phase as well as increased non-specific binding of process- and product-related impurities over the lifetime of the stationary phase.

4. Conclusions

This work provides a comprehensive evaluation of Protein A stationary phases using a panel of mAbs, bsAbs, and Fc-fusion proteins. Morphological properties of stationary phases were characterized using a variety of orthogonal techniques, including TEM, particle sizing, pressure-flow behavior, and isocratic pulse response. These results show highly porous particles with particle diameters consistent with manufacturer's data. Equilibrium isotherms were found to be highly favorable, and EBCs averaged 52–92 mg/mL packed bed across all mAbs and bsAbs for a given stationary phase. EBCs were lower for the larger Fc-fusion proteins, averaging 25–49 mg/mL packed bed. The stationary phases also had high DBCs for mAbs and bsAbs, broadly falling into three groups. The first group of stationary phases (MabSelect SuRe pcc and MabSelect PrismA) had DBCs which averaged 62–66 mg/mL packed bed across all mAbs and bsAbs at 4 min residence times. The next group (KanCapA 3G, Toyopearl AF-rProtein A HC-650F, MabSelect SuRe LX, Praesto AP, and Amsphere A3) averaged 50–53 mg/mL packed bed, and the remaining stationary phases average 39–45 mg/mL packed bed. Groupings of resins were similar for the larger Fc-fusion proteins but DBCs were roughly one third of those determined for mAbs and bsAbs. Effective pore diffusivities were obtained by fitting the general rate model to breakthrough data. The fitted D_e-values for mAbs ranged from $1.1–5.7 \times 10^{-8}$ cm^2/s. Not surprisingly, the larger bsAbs and Fc-fusion proteins showed lower D_e-values.

Elution behavior was evaluated using linear pH gradient elution, and the resulting pH at which elution occurred was nearly identical for all proteins on a given stationary phase except for Fc3, which eluted 0.3–0.5 pH unit higher than all other proteins. Only slight variations in the elution pH were observed between stationary phases, with Toyopearl AF-rProtien A HC-650F requiring a lower pH (~0.3 pH units lower), and MabSpeed rP202 eluting at a higher pH (~0.4 pH units higher). Stationary phases were evaluated in a capture setting using clarified cell culture broth as a feedstock. The resulting product yields were high, while elution pool volumes ranged from 2–3 column volumes in most cases. HCP, DNA, and aggregate levels in the elution pool were dependent on the specific nature of protein being purified, and levels were consistent between stationary phases.

Bivariate correlation analysis was performed to elucidate the relationship between stationary phase morphological properties, protein adsorption, and mass transfer. The results of this analysis demonstrate a linear correlation between EBC and DBC at 4 min residence time across a wide range of proteins and stationary phases. Lastly, our findings suggest as Protein A stationary phase manufacturers trend toward smaller bead sizes to overcome mass transfer limitations, pressure-flow behavior in process-scale columns will have a greater influence on optimization outcomes, particularly for short residence time ranges previously identified by other groups as probable optima.

Conflict of interest statement

The authors declare no conflict of interest. The stationary phases evaluated in this study were purchased commercially or obtained as samples without restrictions on use or publication. No parties external to MedImmune participated in preparation of this manuscript or approved disclosure of its contents.

Acknowledgements

We would like to thank many collaborators at MedImmune for making this work possible; including, Lindsay Arnold, Wai Keen Chung, Chris Thompson, Matt Aspelund, Paul Santacroce, and Chris Afdahl for providing proteins used in this study; Arsala Wallace, Njanma Amadi-Obi, and Jon Borman for analytical testing; and Dana Motabar for review of the manuscript. We thank Al Inman and Robert Keys at Charles River Pathology Associates for TEM imaging. We owe a special thanks to Eric von Lieres and the entire CADET team for making this valuable computational tool available to the scientific community. Lastly, we are very grateful to William Wang (at MedImmune) for his support, encouragement, and detailed review of this manuscript.

Appendix A. Supplementary data

Supplementary data associated with this article can be found, in the online version, at https://doi.org/10.1016/j.chroma.2018.03.060.

References

[1] D.M. Ecker, S.D. Jones, H.J. Levine, The therapeutic monoclonal antibody market, MAbs 7 (2015) 9–14.
[2] U. Brinkmann, R.E. Kontermann, The making of bispecific antibodies, MAbs 9 (2017) 182–212.
[3] C. Sheridan, Despite slow progress, bispecifics generate buzz, Nat. Biotechnol. 34 (2016) 1215–1217.
[4] A. Beck, L. Goetsch, C. Dumomtet, N. Corvaïa, Strategies and challenges for the next generation of antibody–drug conjugates, Nat. Rev. Drug Discov. 16 (2017) 315–337.
[5] S. Hober, K. Nord, M. Linhult, Protein A chromatography for antibody purification, J. Chromatogr. B 848 (2007) 40–47.
[6] S. Ghose, M. Allen, B. Hubbard, C. Brooks, S.M. Cramer, Antibody variable region interactions with Protein A: implications for the development of generic purification processes, Biotech. Bioeng. 92 (2005) 665–673.
[7] S. Ghose, B. Hubbard, S.M. Cramer, Binding capacity differences for antibodies and Fc-fusion proteins on Protein A chromatographic materials, Biotech. Bioeng. 96 (2007) 768–779.
[8] S. Ghose, T. McNerney, B. Hubbard, Protein A affinity chromatography for capture and purification of monoclonal antibodies and Fc-fusion proteins: practical considerations for process development, in: A.A. Shukla, M.R. Etzel, S. Gadam (Eds.), Process Scale Bioseparations for the Biopharmaceutical Industry, CRC, Press, Boca Raton, FL, 2006, pp. 463–490.
[9] S. Vunnum, G. Vedantham, B. Hubbard, Protein A-based affinity chromatography, in: U. Gottschalk (Ed.), Process Scale Purification of Antibodies, John Wiley & Sons, Hoboken, NJ, 2009, pp. 79–102.

[10] A.A. Shukla, B. Hubbard, T. Tressel, S. Guhan, D. Low, Downstream processing of monoclonal antibodies – application of platform approaches, J. Chromatogr. B 848 (2007) 28–39.
[11] B. Kelley, Industrialization of mAb production technology: the bioprocessing industry at a crossroads, MAbs 1 (2009) 443–452.
[12] H.F. Liu, J. Ma, C. Winter, R. Bayer, Recovery and purification process development for monoclonal antibody production, MAbs 2 (2010) 1–20.
[13] A.A. Shukla, L.S. Wolfe, S.S. Mostafa, C. Norman, Evolving trends in mAb production processes, Bioeng. Transl. Med. 2 (2017) 58–69.
[14] M. Urmann, H. Graalfs, M. Joehnck, L.R. Jacob, C. Frech, Cation-exchange chromatography of monoclonal antibodies: characterization of a novel stationary phase designed for production-scale purification, MAbs 2 (2010) 395–404.
[15] Y. Tao, A. Ibraheem, L. Conley, D. Cecchini, S. Ghose, Evaluation of high-capacity cation exchange chromatography for direct capture of monoclonal antibodies from high-titer cell culture processes, Biotechnol. Bioeng. 111 (2014) 1354–1364.
[16] S. Ghose, B. Hubbard, S.M. Cramer, Evaluation and comparison of alternatives to Protein A chromatography mimetic and hydrophobic charge induction chromatographic stationary phases, J. Chromatogr. A 1122 (2006) 144–152.
[17] J. Pezzini, G. Joucla, R. Gantier, M. Toueille, A.-M. Lomenech, C. Le Sénéchal, B. Garbay, X. Santarelli, C. Cabanne, Antibody capture by mixed-mode chromatography: a comprehensive study from determination of optimal purification conditions to identification of contaminating host cell proteins, J. Chromatogr. A 1218 (2011) 8197–8208.
[18] G. Joucla, C. Le Sénéchal, M. Bégorre, B. Garbay, X. Santarelli, C. Cabanne, Cation exchange versus multimodal cation exchange resins for antibody capture from CHO supernatants: Identification of contaminating Host Cell Proteins by mass spectrometry, J. Chromatogr. B 942–943 (2013) 126–133.
[19] M. DiLeo, A. Ley, A.E. Nixon, J. Chen, Choices of capture chromatography technology in antibody manufacturing processes, J. Chromatogr. B 1068–1069 (2017) 136–148.
[20] P. McDonald, C. Victa, L. Franklin-Carter, R. Fahrner, Selective antibody precipitation using polyelectrolytes: a novel approach to the purification of monoclonal antibodies, Biotechnol. Bioeng. 102 (2009) 1141–1151.
[21] Y. Brodsky, C. Zhang, Y. Yigzaw, G. Vedanthan, Caprylic acid precipitation method for impurity reduction: an alternative to conventional chromatography for monoclonal antibody purification, Biotechnol. Bioeng. 109 (2012) 2589–2598.
[22] R. Sommer, A. Tscheilessnig, P. Satzer, H. Schultz, B. Helk, A. Jungbauer, Capture and intermediate purification of recombinant antibodies with combined precipitation methods, Biochem. Eng. J. 93 (2015) 200–215.
[23] A. Azevedo, P.A.J. Rosa, I.F. Ferreira, M.R. Aires-Barros, Chromatography-free recovery of biopharmaceuticals through aqueous two-phase processing, Trends Biotehnol. 27 (2009) 240–247.
[24] D. Platis, N.E. Labrou, Application of a PEG/salt aqueous two-phase partition system for the recovery of monoclonal antibodies from unclarified transgenic tobacco extract, Biotechnol. J. 4 (2009) 1320–1327.
[25] P.A.J. Rosa, A. Azevedo, S. Sommerfeld, M. Mutter, W. Bäcker, M.R. Aires-Barros, Continuous purification of antibodies from cell culture supernatant with aqueous two-phase systems: from concept to process, Biotechnol. J. 8 (2013) 352–362.
[26] G. Bolton, K.K. Mehta, The role of more than 40 years of improvement in Protein A chromatography in the growth of the therapeutic antibody industry, Biotechnol. Prog. 32 (2016) 1193–1202.
[27] H.K. Kim, V. Thammavongsa, O. Schneewind, D. Missiakas, Recurrent infections and immune evasion strategies of *Staphylococcus aureus*, Curr. Opin. Microbiol. 15 (2012) 92–99.
[28] A. Surolia, D. Pain, M.I. Khan, Protein A: nature's universal anti-antibody, Trends Biochem. Sci. 7 (1982) 74–76.
[29] H. Gouda, M. Shiraishi, H. Takahashi, K. Kato, H. Torigoe, Y. Arata, I. Shimada, NMR study of the interaction between the B domain of Staphylococcal Protein A and the Fc portion of Immunoglobulin G, Biochemistry 37 (1998) 129–136.
[30] G. Silverman, B cell superantigens: possible roles in immunodeficiency and autoimmunity, Semin. Immunol. 10 (1998) 43–55.
[31] M. Linhult, S. Gülich, T. Gräslund, A. Simon, M. Karlsson, A. Sjöberg, K. Nord, S. Hober, Improving the tolerance of a Protein A analogue to repeated alkaline exposures using a bypass mutagenesis approach, Proteins: Struct. Funct. Bioinf. 55 (2004) 407–416.
[32] B. Kelley, Very large scale monoclonal antibody purification: the case for conventional unit operations, Biotechnol. Prog. 23 (2007) 995–1008.
[33] M. Trexler-Schmidt, S. Sze-Khoo, A.R. Cothran, B.Q. Thai, S. Sargis, B. Lebreton, B. Kelley, G.S. Blank, Purification strategies to process 5 g/L titers of monoclonal antibodies, Biopharm. Int. (Suppl. March) (2009).
[34] M. Freiherr von Roman, S. Berensmeier, Improving the binding capacities of Protein A chromatographic materials by means of ligand polymerization, J. Chromatogr. A 1347 (2014) 80–86.
[35] E. Müller, J. Vajda, Routes to improve binding capacities of affinity resins demonstrated for Protein A chromatography, J. Chromatogr. B 1021 (2016) 159–168.
[36] J.T. McCue, G. Kemp, D. Low, I. Quinones-García, E valuation of protein-A chromatography media, J. Chromatogr. A 989 (2003) 139–153.
[37] R. Hahn, R. Schlegel, A. Jungbauer, Comparison of Protein A affinity sorbents, J. Chromatogr. B 790 (2003) 35–51.
[38] R. Hahn, P. Bauerhansl, K. Shimahara, C. Wizniewski, A. Tscheliessnig, A. Jungbauer, Comparison of Protein A affinity sorbents: II. Mass transfer properties, J. Chromatogr. A 1093 (2005) 98–110.
[39] E.X. Perez-Almodovar, G. Carta, IgG adsorption on a new protein A adsorbent based on microporous hydrophilic polymers, I. Adsorption equilibrium and kinetics, J. Chromatogr. A 1216 (2009) 8339–8347.
[40] Z. Liu, S.S. Mostafa, A.A. Shukla, A comparison of Protein A chromatographic stationary phases: performance characteristics for monoclonal antibodies, Biotechnol. Appl. Biochem. 62 (2015) 37–47.
[41] S. Schweiger, S. Hinterberger, A. Jungbauer, Column-to-column packing variation of disposable pre-packed columns for protein chromatography, J. Chromatogr. A 1527 (2017) 70–79.
[42] R.B. Bird, W.E. Stewart, E.N. Lightfoot, Transport Phenomena, Wiley, New York, 1960.
[43] L. Hagel, M. Ostberg, T. Andersson, Apparent pore size distributions of chromatography media, J. Chromatogr. A 743 (1996) 33–42.
[44] P.G. Squire, Calculation of hydrodynamic parameters of random coil polymers from size exclusion chromatography and comparison with parameters by conventional methods, J. Chromatogr. 210 (1981) 433–442.
[45] C.K.S. Ng, H. Osuna-Sanchez, E. Valéry, E. Sørensen, D.G. Bracewell, Design of high productivity antibody capture by protein A chromatography using an integrated experimental and modeling approach, J. Chromatogr. B 899 (2012) 116–126.
[46] C.K.S. Ng, F. Rousset, E. Valéry, D.G. Bracewell, E. Sørensen, Design of high productivity sequential multi-column chromatography for antibody capture, Food Bioprod. Process. 92 (2014) 233–241.
[47] J.M. Reck, T.M. Pabst, A.K. hunter, G. Carta, Separation of antibody monomer-dimer mixtures by frontal analysis, J. Chromatogr. A 1500 (2017) 96–104.
[48] E. von Lieres, J. Andersson, A fast and accurate solver for the general rate model of column liquid chromatography, Comput. Chem. Eng. 34 (2010) 1180–1191.
[49] https://github.com/modsim/CADET.
[50] G. Carta, A. Jungbauer, Protein Chromatography, 1st ed., Wiley-VCH, Germany, 2010, pp. 75–76.
[51] B.D. Bowes, A.M. Lenhoff, Protein adsorption and transport in dextran-modified ion-exchange media. II. Intraparticle uptake and column breakthrough, J. Chromatogr. A 1218 (2011) 4698–4708.
[52] J.J. Carberry, A boundary-layer model of fluid-particle mass transfer in fixed beds, AIChE J. 6 (1960) 460–463.
[53] A.A. Shukla, P. Gupta, X. Han, Protein aggregation kinetics during Protein A chromatography: case study for an Fc fusion protein, J. Chromatogr. A 1171 (2007) 22–28.
[54] T.M. Pabst, R. Palmgren, A. Forss, J. Vasic, M. Fonseca, C. Thompson, W.K. Wang, X. Wang, A.K. Hunter, Engineering of novel Staphylococcal Protein A ligands to enable milder elution pH and high dynamic binding capacity, J. Chromatogr. A 1362 (2014) 180–185.
[55] S. Gülich, M. Ulhén, S. Hober, Protein engineering of an IgG-binding domain allows milder elution conditions during affinity chromatography, J.Biotechnol. 76 (2000) 233–244.
[56] N.L. Brown, S.P. Bottomley, M.D. Scawen, M.G. Gore, A study of the interactions between an IgG-binding domain based on the B domain of Staphylococcal Protein A and rabbit IgG, Mol. Biotechnol. 10 (1998) 9–16.
[57] H. Watanabe, H. Matsumaru, A. Ooishi, S. Honda, Structure-based histidine substitution for optimizing pH-sensitive *Staphylococcus* protein A, J. Chromatogr. B 929 (2013) 155–160.
[58] A.A. Shukla, P. Hinckley, Host cell protein clearance during Protein A chromatography: development of an improved column wash step, Biotechnol. Prog. 24 (2008) 1115–1121.
[59] B. Nogal, K. Chhiba, J.C. Emery, Select host cell proteins coelute with monoclonal antibodies in Protein A chromatography, Biotechnol. Prog. 28 (2012) 454–458.
[60] N. Aboulaich, W.K. Chung, J. Heidbrink Thompson, C. Larkin, D. Robbins, M. Zhu, A novel approach to monitor clearance of host cell proteins associated with monoclonal antibodies, Biotechnol. Prog. 30 (2014) 1114–1124.
[61] E.X. Perez-Almodovar, G. Carta, IgG adsorption on a new protein A adsorbent based on microporous hydrophilic polymers. II. Pressure–flow curves and optimization for capture, J. Chromatogr. A 1216 (2009) 8348–8354.
[62] K. Swinnen, A. Krul, I. Van Goidsenhoven, N. Van Tichelt, A. Roosen, K. Van Houdt, Performance comparison of protein A affinity resins for the purification of monoclonal antibodies, J. Chromatogr. B 848 (2007) 97–107.
[63] V. Girard, N. Hilbold, C.K.S. Ng, L. Pegon, W. Chahim, F. Rousset, V. Monchois, Large-scale monoclonal antibody purification by continuous chromatography, from process design to scale-up, J. Biotechnol. 213 (2015) 65–73.
[64] J.J. Stickel, A. Fotopoulos, Pressure-flow relationships for packed beds of compressible chromatography media at laboratory and production scale, Biotechnol. Prog. 17 (2001) 744–751.
[65] J.T. McCue, D. Cecchini, C. Chu, W. Liu, A. Spann, Application of a two-dimensional model for predicting the pressure-flow and compression properties during column packing scale-up, J. Chromatogr. A 1145 (2007) 89–101.
[66] R.N. Keener III, E.J. Fernandez, J.E. Maneval, R.A. Hart, Advancement in the modeling of pressure-flow for the guidance of development and scale-up of commercial-scale biopharmaceutical chromatography, J. Chromatogr. A 1190 (2008) 127–140.

[67] H. Luo, N. Lee, X. Wang, Y. Li, A. Schmelzer, A.K. Hunter, T. Pabst, W.K. Wang, Liquid-liquid phase separation causes high turbidity and pressure during low pH elution process in Protein A chromatography, J. Chromatogr. A 1488 (2017) 57–67.
[68] R. Hahn, K. Shimahara, F. Steindl, A. Jungbauer, Comparison of protein A affinity sorbents III. Life time study, J. Chromatogr. A 1102 (2006) 224–231.
[69] C. Jiang, J. Liu, M. Rubacha, A.A. Shukla, A mechanistic study of Protein A chromatography resin lifetime, J. Chromatogr. A 1216 (2009) 5849–5855.
[70] A. Grönberg, M. Eriksson, M. Ersoy, H.J. Johansson, A tool for increasing the lifetime of chromatography resins, mAbs 3 (2011) 192–202.
[71] S. Zhang, W. Daniels, J. Salm, J. Glynn, J. Martin, C. Gallo, R. Godavarti, G. Carta, Nature of foulants and fouling mechanism in the Protein A MabSelect resin cycled in a monoclonal antibody purification process, Biotechnol. Bioeng. 113 (2016) 141–149.
[72] S. Zhang, K. Xu, W. Daniels, J. Salm, J. Glynn, J. Martin, C. Gallo, R. Godavarti, G. Carta, Structural and functional characteristics of virgin and fouled Protein A MabSelect resin cycled in a monoclonal antibody purification process, Biotechnol. Bioeng. 113 (2016) 367–375.
[73] M. Pathak, A.S. Rathore, Mechanistic understanding of fouling of protein A chromatography resin, J. Chromatogr. A 1459 (2016) 78–88.